CARBON letters

Original Articles
Carbon Letters Vol. 27, 26-34 (2018)

Assembly of chemically reduced graphene oxide with folic acid functionalized with pyrene moieties and electrochemical sensing of folate receptors

Binhee Kwon[1], Jongyeap Park[1], Woojun Jeong[1], Guembi Jeong[1], Hyeong Seon Ryu[2], Peerasak Paoprasert[3,♠], Sung Young Park[1,4,♠] and Insik In[1,5,♠]

Article Info

Received 6 November 2017
Accepted 11 December 2017

♠Corresponding Author

E-mail: peerasak@tu.ac.th
E-mail: parkchem@ut.ac.kr
E-mail: in1@ut.ac.kr
Tel: +66-88-610-3311
Tel: +82-43-841-5225
Tel: +82-43-841-5422

Open Access

DOI: http://dx.doi.org/10.5714/CL.2018.27.026

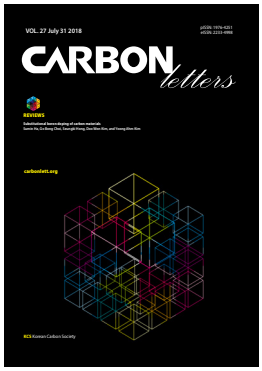

http://carbonlett.org

pISSN: 1976-4251
eISSN: 2233-4998

[1]Department of IT Convergence (Brain Korea PLUS 21), Korea National University of Transportation, Chungju 27469, Korea
[2]Department of Organic and Nano Engineering, Hanyang University, Seoul 04763, Korea
[3]Department of Chemistry, Faculty of Science and Technology, Thammasat University, Pathumthani 12121, Thailand
[4]Department of Chemical and Biological Engineering, Korea National University of Transportation, Chungju 27469, Korea
[5]Department of Polymer Science and Engineering, Korea National University of Transportation, Chungju 27469, Korea

Abstract

To formulate folate receptor (FR)-specific graphene-based electrochemical electrodes, a folic acid (FA) derivative attached with two pyrene molecules on the glutamate tail of FA was synthesized. The resulting pyrene-functionalized FA (FA-Py) presented the spontaneous noncovalent binding on chemically reduced graphene oxides (rGO) through an π-π interaction. Ultrathin morphology, high water-resistance, and preservation of intact FR-specific pteroates from the rGO/FA-Py assembly allow this assembly to be exploited as robust and FR-specific electrochemical electrode materials. The limits of detecting rGO/FA-Py modified electrodes were found to be as low as 3.07 nM in FR concentrations in cyclic voltammetry analysis.

Key words: chemically reduced graphene oxide, noncovalent interaction, electrochemical sensing, folic acid, folate receptor

1. Introduction

Two-dimensional (2D) graphene has received intensive academic and industrial interests due to its outstanding electrical, thermal, and mechanical performances [1,2]. While a bottom-up approach can produce high quality graphene thin films applicable to transistors or transparent conductors [3], a top-down approach that utilizes graphene oxide (GO) is becoming more important because the mass production of graphene-based nanomaterials or nanocomposites is easily feasible in this approach [4,5]. In the top-down approach, chemically reduced GO (rGO) that has certain amounts of oxidized carbon through the graphene framework is typically produced from GO by various reducing reactions [6]. To provide solution processability to rGO, the functionalization of either GO or rGO is inevitable to minimize a strong van der Waals force-mediated interlayer adhesion of rGO sheets [7,8]. Numerous noncovalent functionalization methods have been exploited to produce soluble rGO assemblies or hybrids with various small molecules or polymers [9,10]. The $-\pi$ or $\pi-\pi$ interaction between organic molecules (including polymers) and π–rich rGO not only offers high dispersion stability, but also incorporates the target-specific function to rGO for various

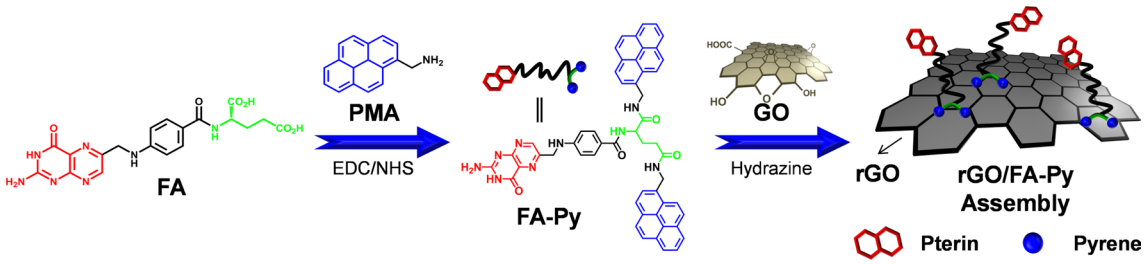

Fig. 1. Illustration of the synthesis of FA-Py from FA and PMA (red, green, blue colored parts are pterin, glutamate, and pyrene moieties, respectively).

practical applications [11-15].

Therefore, it is highly motivating to apply this noncovalent functionalization method to construct an rGO assembly with precisely designed molecular structures and target-specific functions. In this study, noncovalent conjugation of folic acid (FA) on rGO was attempted by synthesizing pyrene-conjugated FA and noncovalently attaching the prepared pyrene-conjugated FA on rGO through an π–π interaction between pyrene moieties and rGO plates to formulate folate receptor (FR)-specific graphene hybrid electrode materials. While direct noncovalent functionalization of FA molecules on rGO has been successfully attempted through a noncovalent functionalization method in the previous study [15], direct anchoring of functional organic molecules on rGO might be detrimental in implementing the original activity of pristine functional organic molecules. In particular, the precise controlling of σ–π interactions between σ-rich molecules (or polymers) and π-rich rGO is very difficult because even the defining and manipulation of interacting interfaces between the σ-rich organic molecules and π-rich rGO is hardly attainable. Theoretically, multiple modes of noncovalent interactions have been demonstrated by the molecular simulations during the noncovalent binding of small molecules such as lysine on graphene [16]. Few experimental studies have also proven the slight perturbation of pristine functions of organic molecules after noncovalent binding on the rGO plates. It has been reported that noncovalently prepared heparin (high molecular weight)/rGO conjugates present only 35% preservation of blood anti-clotting performance compared with the free heparin [11]. Controlling the relative mass ratio of σ-rich polymers and π-rich rGO can also induce the morphological variation of noncovalently interacting polymers on the rGO plates. Both the "side-by-face" or "end-by-face" interacting modes of poly(*N*-isopropyl acrylamide) (PNIPAm) binding on rGO have been proposed to explain the modulation of the lower critical solution temperature of PNIPAm/rGO assemblies depending on the feeding ratio between PNIPAm and rGO in the assemblies [13]. Therefore, the proper designing of noncovalent binding modes between the organic molecules and graphene-based nanomaterials is a prerequisite for accomplishing the performance maximization of noncovalently interacting organic molecules.

FA moieties can be widely acceptable as a structural component for the designing of various cancer cell-specific nanocarriers or nanosensors through the robust and specific molecular recognition between FA and FR [17]. For the molecular design of FR-specific graphene-based electrodes, the incorporation of pyrene moieties into FA was attempted with the glutamate tails of FAs. While FA is composed of both a pteroate head (pterin and aminobenzoate moieties) and a glutamate tail, it has been reported that a positive pteroate head was strongly anchored inside of the negatively charged pocket of FR during the molecular recognition process between FA and FR [18]. Then, the glutamate tails stretched out of the molecular pockets of FRs. Therefore, the functionalization of pyrene moieties with the glutamate tails of FAs was attempted to minimize the possible retardation of the molecular recognition process between the FRs and pteroate heads of FAs. The resulting FA functionalized with two pyrene moieties on its glutamate tail (FA-Py) possesses both a FR-specific pteroate head (through molecular recognition) and graphene-anchorable pyrene groups (through π-π interaction) (Fig. 1). The designing and utilization of FA-Py in this study can be very advantageous for developing FR- or cancer cell-specific graphene based nanohybrids or electrodes, as shown in this study. The noncovalent hybridization of FA-Py on rGO can be easily attempted by the simple mixing of both FA-Py and GO and the subsequent chemical reduction of the FA-Py/GO mixture to the FA-Py/rGO assembly, as shown in other studies [9,10]. Finally, the FA-Py/rGO assembly can be effectively utilized as FR- or cancer cell-specific electrochemical electrode materials, which are very critical for the in-vitro cancer diagnosis, especially in the early stages of cancer.

2. Experimental

2.1. Materials and characterization

FA (≥97%, #F7876), 1-pyrenemethylamine hydrochloride (PMA; 95%, #401633), ethyl(dimethylaminopropyl) carbodiimide (EDC; ≥97%, #39391), *N*-hydroxysuccinimide (NHS; 98%, #130672), 64–65% hydrazine monohydrate (98%, #207942), dimethylformamide (DMF; 99.8%, #319937), and folate receptor 2 human recombinant (FR, ≥95%, #F7057) were purchased from Sigma-Aldrich Corp (USA). Anodized aluminum oxide (AAO) membrane (Whatman, diameter of 47 mm and pore size of 0.2 μm) was purchased from the Fischer Scientific Corp.

Ultraviolet-visible (UV-Vis) spectra were obtained with an Optizen Alpha UV-Vis Smart Spectrometer of Mecasys (Korea). The photoluminescence (PL) spectra were obtained from a FluoroMate FS-2 luminescence spectrometer of Scinco (Korea). The Fourier transform infrared (FT-IR) spectra were taken with a FT/

IR-4600 of Jasco, Inc (USA). Transmission electron microscopy (TEM) images were obtained from a Tecnai G2 F20 field emission transmission electron microscope of the FEI Corporation (USA). Proton nuclear magnetic resonace (^{1}H-NMR) spectra were obtained using a Bruker Advance 400 MHz spectrometer (Germany) with deuteriated dimethyl sulfoxide (DMSO-d_6) as the solvent. PL decay profiles were obtained with the FL920 of Edinburgh, Inc. Atomic force microscope (AFM) images were obtained using a Multimode-N3-AM Scanning Probe Microscope of Bruker. X-ray photoelectron spectroscopy (XPS) spectra were obtained by using a tetra probe base system (Thermo Fisher Scientific Co.). X-ray diffraction (XRD) patterns were obtained with D8 Advance of Bruker with 1.54059 Å Cu Kα 1 as the wavelength. Raman analysis was done with ARAMIS of Horiba Jobin Yvon (France) with a laser wavelength of 532 nm. Field-effect scanning electron microscope (FE-SEM) images were obtained with SNE-4500 of SEC. Cyclic voltammetry (CV) measurements were obtained from Autolab PGSTAT12 of Metrohm.

2.2. Synthesis of FA-Py

FA-Py was synthesized by an amidation reaction between FA and PMA. At first, both the FA (1 eqv.) and PMA (10 eqv.) were dissolved in 150 mL of DMF/pyridine (volume ratio of 2:1) mixed solvent in a one neck round bottom flask. Then, EDC (10 eqv.) and NHS (20 eqv.) were added into the above mixture and the mixture solution was heated at 35°C for 72 h. Afterwards, in order to remove any remaining EDC, NHS, and PMA from the crude FA-Py, the entire reaction mixture was diluted with 40 mL of additional DMF and poured into excess amounts of methanol where all EDC, NHS, and PMA are highly soluble. The brown precipitation was isolated by vacuum filtration and sequential washing with a plentiful amount of buffer (pH 10) where any free FA is highly soluble. Finally, purified FA-Py powders were obtained after vacuum drying at 40°C for 24 h with a mass yield of 79.6%.

2.3. Synthesis of rGO/FA-Py assembly

A soluble rGO/FA-Py assembly was prepared from the chemical reduction of the mixture solution of GO (1 mg in 1 mL of water) and FA-Py (1 mg in 25 mL of DMF) by 10 μL of hydrazine monohydrate at 80°C for 24 h. An initially bright brown GO/FA-Py mixture solution was changed to a dark black rGO/FA-Py assembly solution. Purified assembly powders were obtained after ultracentrifugating the crude assembly solution at 7041 rcf (relative centrifugal force) and the sequential vacuum drying of precipitates at 30°C for 24 h. rGO/FA-Py assembly powders are soluble in DMF with the help of a brief tip sonication (Q700 sonicator with maximum power of 700 W at 20 kHz) with 20% of maximum powder for 20 min.

2.4. Electrochemical sensing of FRs

CV analysis was attempted with three electrode systems comprised of a counter electrode (platinum wire), reference electrode (Ag/AgCl, SCE), and working electrode (glassy carbon electrode [GCE], diameter of 3 mm) in 10 mM of $K_3[Fe(CN)_6]$ containing 100 mM of KCl as the electrolyte. Firstly, GCE was slightly rubbed with alumina powders and gently sonicated by tip sonication for surface cleaning. Secondly, 5 μL of the rGO/FA-Py assembly solution (1 mg mL^{-1} in DMF, briefly tip sonicated just before dropping) was slowly dropped on the active area of GCE, and the resulting rGO/FA-Py modified GCE electrode was dried in a vacuum oven. The CV response of the electrodes was observed from –0.2 to 0.7 V at a scan speed of 100 mV s^{-1}, and the current was changed between –50 μA and +40 μA. Identical CV measurements were attempted with or without FRs with different concentrations (5, 10, 25, 50 nM) in the aqueous electrolyte solution.

3. Results and Discussion

Pyrene, one of the well-known molecular linkers that can spontaneously anchor on graphene or rGO plates through π–π interactions, was covalently attached with the glutamate tail of FA. The amidation of FA with excess PMA in the DMF/pyridine mixture solution produced FA-Py with a high mass yield. The purification of FA-Py was successfully attempted by exploiting the different solubilities of starting reagents and FA-Py. Both the ^{1}H-NMR and FT-IR analysis (Supplementary Figs. S1 and S2) clearly supported the successful synthesis of FA-Py where two Py moieties are present in each FA-Py. The use of lower amounts of PMA produced a mixture of mono-substituted byproducts and FA-Py after synthesis, but the separation of this mixture into each compound was practically impossible due to the similar organic solubility of both.

Then the noncovalent functionalization of FA-Py with rGO was examined through the chemical reduction of GO to rGO and the simultaneous noncovalent binding of FA-Py on rGO, which forms a stable rGO/FA-Py assembly. Because FA-Py is only soluble in polar aprotic solvents such as DMF and DMSO, the formation of the rGO/FA-Py assembly was attempted, not in aqueous media, but in a DMF/H_2O (9:1) mixture solvent according to the previous reports [19]. After chemical reduction, the initially pale-brown GO/FA-Py mixture solution turned into a dark-black rGO/FA-Py assembly solution (Fig. 2a). The prepared rGO/FA-Py assembly was highly dispersible in solvent media such as DMF, and no floating particles or precipitates were observed, even after 6 mo. This shows that the noncovalent functionalization of FA-Py on rGO through π-π interactions between the pyrene moieties of FA-Py and rGO proceeded well in our study.

The UV-Vis spectrum of the rGO/FA-Py assembly showed that the optical absorbance of the assembly significantly increased over the entire wavelength range (Fig. 2a). This confirms that the restoration of the π-conjugation occurred significantly after the chemical reduction [20]. Both the strong absorption peaks at 277, 329, and 345 nm and the weak absorption peaks at 268 and 287 nm presented in the UV-Vis spectrum of both PMA and FA-Py (due to the presence of pyrene moieties in these materials [Supplementary Fig. S3]) were well preserved in the UV-Vis spectrum of both the GO/FA-Py mixture and rGO/FA-Py assembly solutions. The FT-IR spectrum of the rGO/FA-Py assembly films obtained after vacuum filtrating the assembly solution through the AAO membrane showed a loss in the C=O

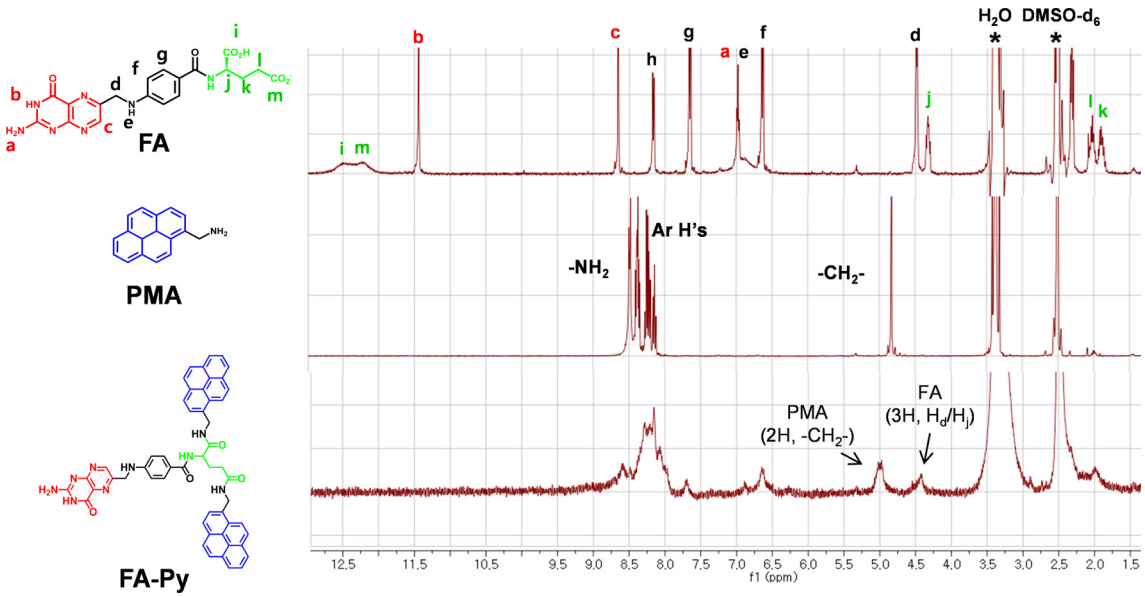

Supplementary Fig. S1. ^{1}H-NMR spectra of FA, PMA and FA-PMA in DMSO-d_6. The number of Py units in FA-Py was calculated from the following equation. The measured integration ratio between the benzyl protons of PMA and H_d/H_j protons of FA in FA-Py is 3:4.1, which closely matches the integration ratio of 3:4 when two Py units are attached to a single FA. Therefore, the attachment of two Py units to the glutamate tail of FA is supposed in FA-Py throughout our study.

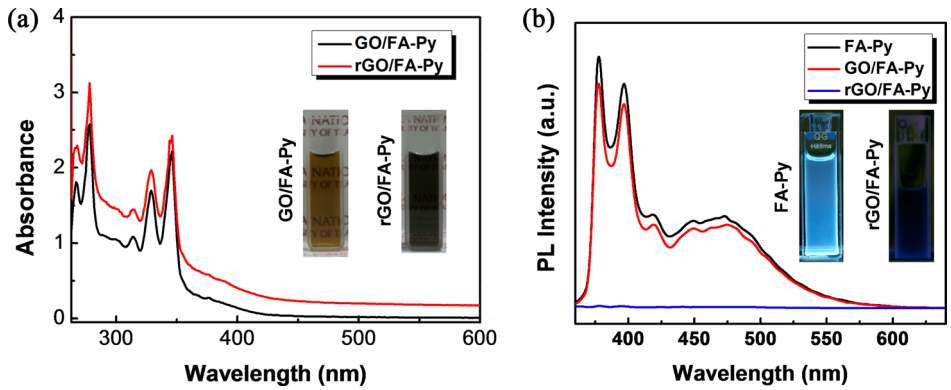

Fig. 2. (a) UV-Vis spectra of rGO/FA-Py and (b) PL spectra of FA-Py, GO/FA-Py (1:10) mixture, and rGO/FA-Py (1:10) assembly (the insets are photo images of FA-Py and rGO/FA-Py assembly solutions in the dark under 365 nm UV lamp).

stretching peak at 1693 cm^{-1}, which was clearly present in the FT-IR spectrum of GO, thereby showing the effective chemical reduction from GO to rGO, even in a mixed solvent system as in this study (Supplementary Fig. S4) [21]. The XPS analysis of the rGO/FA-Py assembly revealed the inclusion of 76.9, 14.7, and 8.4 at% inclusion of carbon, oxygen, and nitrogen elements, respectively (Supplementary Fig. S5). The rGO/FA-Py also revealed an increased C/O ratio of 5.23:1 compared with 2.07:1 in the case of GO, which again shows that the chemical reduction from GO to rGO is facile. The relative ratio of C−C/C=C binding peaks at 284.7 eV compared with the binding peaks of oxidized carbons at 285.3 (C−OH), 286.5 (C−O−C), 288.0 (C=O−NH), and 289.5 eV (C=O−OH), respectively, reached 2.55:1 in a high resolution XPS C1s binding peak after deconvolution (Supplementary Fig. S6). Considering that the relative ratio of graphitic carbon binding peaks to the oxidized carbon binding peaks of GO is typically 1:1 in similar XPS analysis [22], the increased portion of C−C/C=C binding peaks in the rGO/FA-Py assembly again supports the successful progress of chemical reduction from GO to rGO. Also, the occurrence of C−N binding peaks at 285.9 (C−N sp^2) and 287.2 eV (C−N sp^3) clearly supports the presence of FA-Py in the assembly because these binding peaks are also observed in the high resolution XPS C1s binding peak of FA-Py after deconvolution (Supplementary Fig. S7).

As the FA-Py shows a strong fluorescence at 378 and 396 nm, which originated from the monomer emission, and a broad fluorescence centered at 475 nm, which originated from the excimer emission upon UV irradiation due to the presence of two pyrene groups in FA-Py (Supplementary Fig. S8) [23,24], the exploiting of the fluorescence behavior of rGO/FA-Py assembly

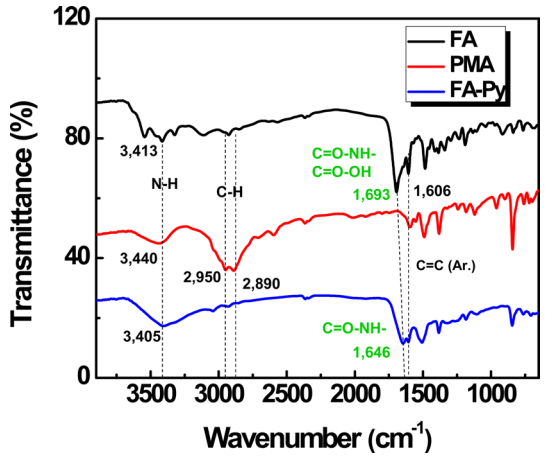

Supplementary Fig. S2. FT-IR (KBr pellet) spectra of FA, PMA and FA-PMA. The attachment of FA units in FA-Py is confirmed by observing the presence of both C=O and C=C (aromatic) stretching peaks at 1646 and 1606 cm^{-1} in the FT-IR spectrum of FA-Py. Because FA-Py does not have carboxylic acid groups, the carbonyl stretching peak of FA at 1693 cm^{-1} (probably both amide and carboxylic acid C=O stretching) shifts to 1646 cm^{-1} (amide C=O stretching).

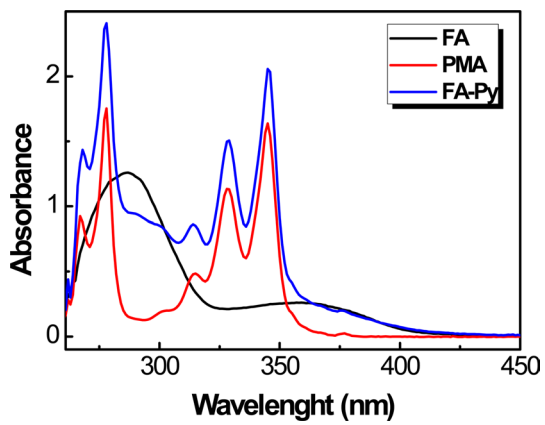

Supplementary Fig. S3. UV-Vis spectra of FA, PMA, and FA-Py in the DMF/H2O (9:1) mixture solvents. The molar concentrations of all samples are equal to 2.52×10^{-5} mol L^{-1}.

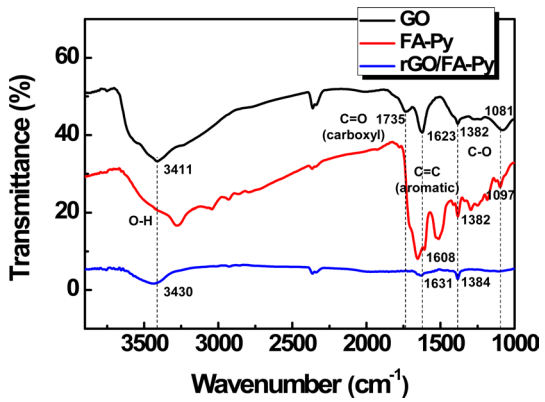

Supplementary Fig. S4. FT-IR (KBr pellet) spectra of GO, FA-PMA and rGO/FA-PMA.

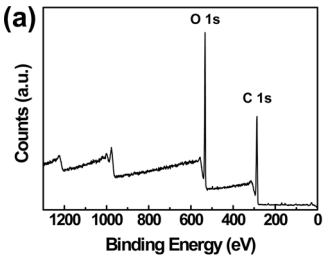

Binding Peak	Binding Energy (eV)	Atomic % (At.-%)
C 1s	287.22	65.75
O 1s	533.13	31.7
C:O ratio		2.07:1

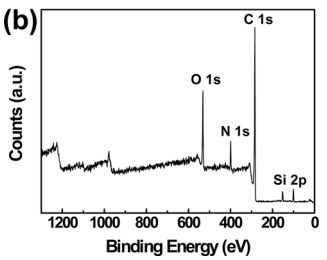

Binding Peak	Binding Energy (eV)	Atomic % (At.-%)
C 1s	284.1	72.2
O 1s	531.3	13.8
N 1s	399.1	7.87
Si 2p	100.8	6.13
C:O ratio		5.23:1

Supplementary Fig. S5. XPS survey scan of rGO/FA-Py assembly. Si binding peak originates from the underlying Si wafer.

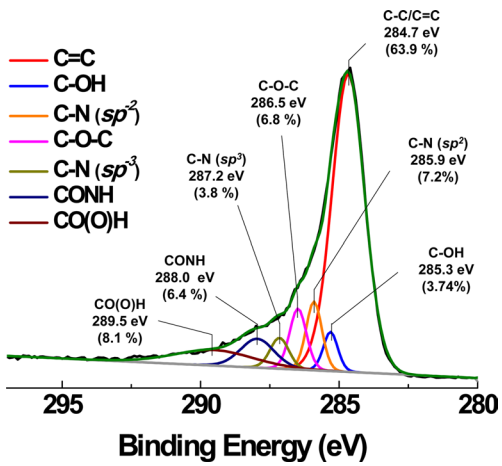

Supplementary Fig. S6. High resolution XPS C1s binding peak of rGO/FA-Py.

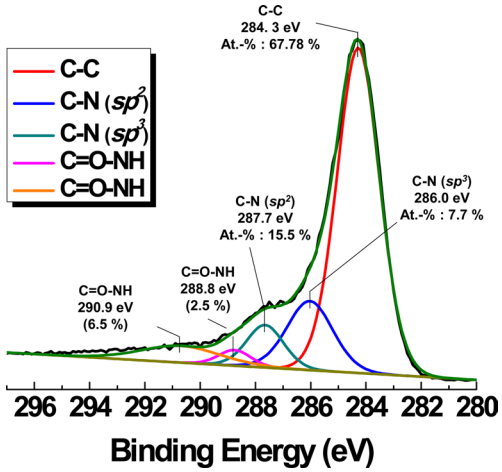

Supplementary Fig. S7. High resolution XPS C1s binding peak of FA-Py.

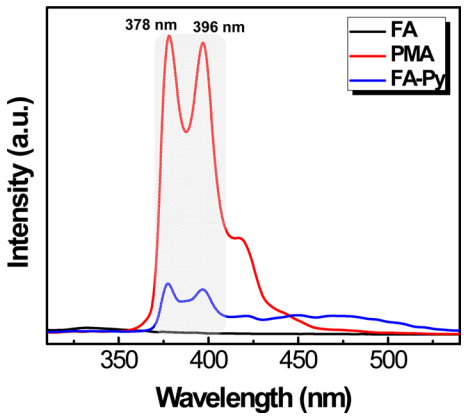

Supplementary Fig. S8. UV-Vis spectra of FA, PMA, and FA-Py in DMF/H2O (9:1) mixture solvents. The molar concentrations of all samples are equal to 1.51×10^{-6} mol L^{-1}.

is very useful to understand the detailed π–π interactions between FA-Py and rGO. While the GO/FA-Py mixture also shows a slight fluorescence quenching compared with FA-Py due to the presence of isolated quasi-graphene domains, even in GO, and the subsequent weak π–π interaction between FA-Py and GO, as reported in other reports [25,26], the rGO/FA-Py assembly presented a nearly complete fluorescence quenching at 378, 396, and 475 nm (Fig. 2b). The efficient fluorescence quenching of FA-Py in the assembly reveals that the spontaneous anchoring of FA-Py on rGO through π–π interaction is highly specific and robust. Previous theoretical calculations have reported that graphene can exhibit significant fluorescence quenching through a long range resonance energy transfer with pyrene moieties when pyrene is placed within distances less than 30 nm from graphene [27]. Therefore, it is regarded that most of the pyrene moieties of noncovalently binding FA-Py molecules closely interact on the surface of rGO. While the rGO/FA-Py assembly shows efficient fluorescence quenching, the fluorescence decay profiles of the assembly can be traced from the weak fluorescence signals of the assembly. The average fluorescence decay time (τ_{avg}) of both the FA-Py and GO/FA-Py mixtures was 1.56 and 1.44 ns, respectively, for the emission of 444 nm from the excitation of 375 nm. Along with the dominant fast decay time (τ_1) of 1.48 (98.5%) and 1.36 ns (97.9%), the minor slower decay time (τ_2) of 6.84 (1.5%) and 5.28 ns (2.1%) was also observed for the FA-Py and GO/FA-Py mixtures, respectively (Supplementary Fig. S9). In the case of the rGO/FA-Py assembly, a much larger τ_{avg} of 1.98 ns was observed along with the increased contribution (8.4%) of τ_2 (4.94 ns) to τ_{avg}. The increased τ_{avg} of the rGO/FA-Py assembly might originate because the efficient fluorescence quenching in the assembly is mediated by the Förster energy transfer from FA-Py to rGO [28].

The morphological features of the rGO/FA-Py assembly were examined by AFM, TEM, and FE-SEM analysis. The AFM image of the rGO/FA-Py assembly revealed a 2D planar sheet-like morphology with a uniform thickness of 1.7 nm (Fig. 3a). Considering the fact that the thickness of GO or rGO is about 1 nm [29], it is estimated that the assembly possesses a single rGO sheet in the middle together with a 0.7 nm-thick surrounding layer of FA-Py molecules on it. An ultrathin sheet-like structure

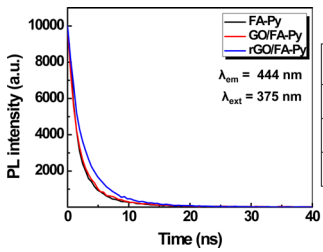

	τ_{avg}	τ_1 (ns)	τ_2 (ns)	R-Square
FA-Py	1.56	6.84 (1.5 %)	1.48 (98.5 %)	0.99845
GO/FA-Py	1.44	5.28 (2.1 %)	1.36 (97.9 %)	0.99963
rGO/FA-Py	1.98	4.94 (8.4 %)	1.71 (91.6 %)	0.99954

Supplementary Fig. S9. Fluorescence decay profiles and average fluorescence decay time of FA-Py, GO/FA-Py mixture, and rGO/FA-Py assembly.

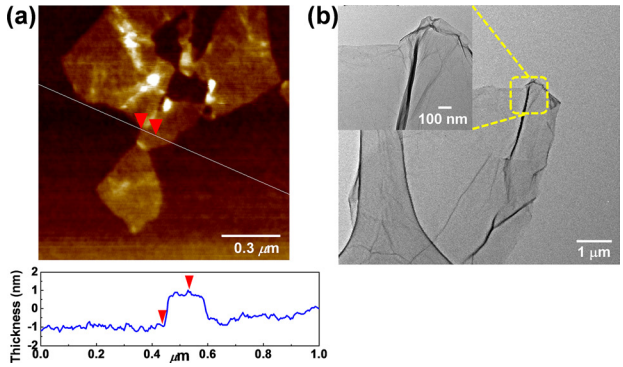

Fig. 3. (a) AFM image of rGO/FA-Py and (b) TEM image of rGO/FA-Py.

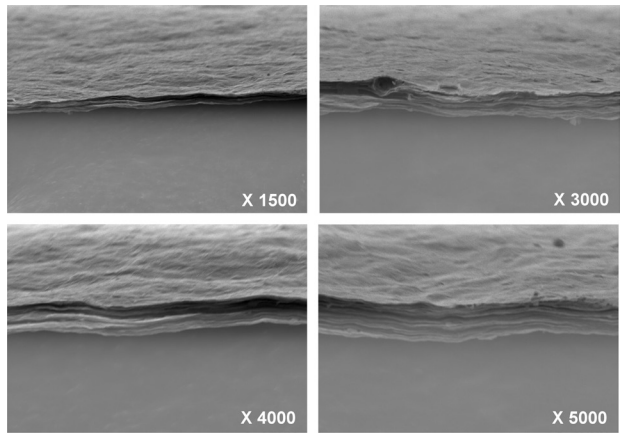

Supplementary Fig. S10. FE-SEM images of rGO/FA-Py assembly films with different magnifications.

of the assembly was again clearly confirmed in TEM analysis, and the typical scrolled/wrinkled morphology of a single rGO sheet was clearly identified (Fig. 3b) [11-15]. Multiple layered rGO sheets were not observed, again showing that the rGO/FA-Py assembly is organized with a single rGO sheet with surrounding FA-Py molecules. The lateral dimension of the rGO/FA-Py assembly spanned from several hundred nm to 5 μm. Due to this laterally large and vertically ultrathin nature of an individual rGO/FA-Py assembly, the film of the assemblies showed a significant vertical stacking of rGO sheets, which is typically observed in the side-view FE-SEM images of GO or rGO (Supplementary Fig. S10) [9].

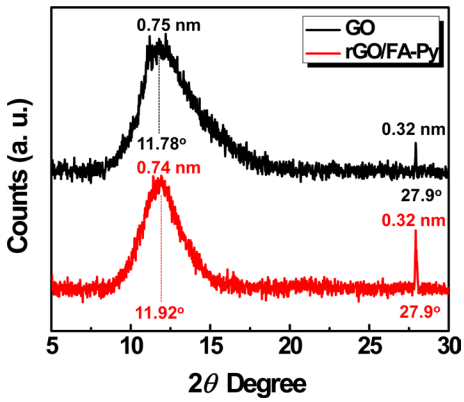

Supplementary Fig. S11. XRD spectra of GO and rGO/FA-Py assembly (1.54059 Å Cu Kα 1 as wavelength).

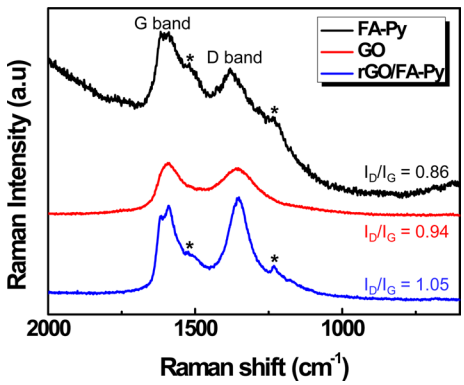

Supplementary Fig. S12. The Raman signatures for FA-Py, GO, and rGO/FA-Py assembly.

The XRD patterns of both GO and rGO/FA-Py were very similar. In addition to the small peaks of graphitic *d*-spacing peaks at 27.9° (0.32 nm), the broad scattering peaks centered at 11.8 and 11.9° were observed, which correspond to the *d*-spacing values of 0.75 and 0.74 nm for the GO and rGO/FA-Py assemblies, respectively (Supplementary Fig. S11) [30]. It is clearly estimated that the van der Waals force- or π–π interaction-mediated aggregation of the neighboring rGO sheets was effectively suppressed in the assembly due to the presence of surrounding FA-Py molecules noncovalently functionalized on the rGO plate. The Raman scattering of the rGO/FA-Py assembly showed clear D and G band peaks at 1351 and 1588 cm^{-1}, respectively (Supplementary Fig. S12). The D to G band peak intensity ratio (I_D/I_G) slightly increased from 0.94 for GO to 1.05 for the assembly, showing that the lateral dimension of the assembly slightly decreased compared with GO. Accordingly, the defect density originating from the sp^3 carbons that are possibly present in the edges of the plate slightly increased [11-15]. Also, the rGO/FA-Py assembly presented the characteristic shoulder Raman peaks of FA-Py at 1233, 1524, 1615 cm^{-1}, which again support the presence of noncovalently functionalized FA-Py molecules in the assembly film.

The ease of preparation, large lateral dimension, ultrathin thickness, and even high water insolubility of rGO/FA-Py assembly prompt us to investigate the application of the assembly as electrode materials for the electrochemical biosensing of FRs highly expressed in cancer cells [31]. In particular, the high binding affinity between FA and FR is known to be based on the incorporation of the pteroate head group of FA rather than the glutamate tail group into the binding pocket of FR [18]. In FA-Py, two pyrene moieties are bound to the glutamate tail of FA, which might not interfere with the specific binding between the pteroate head group of FA in the assembly and FR. After the drop casting of the DMF solution of the rGO/FA-Py assembly on a glassy carbon working electrode, CV analysis presented a peak oxidation current ($i_{p,c}$) of 44.3 μA in an electrochemical cell containing both $K_3[Fe(CN)_6]$ and KCl as electrolytes (Fig. 4a). Then, different amounts of FRs were added into the electrolyte solution and the change of $i_{p,c}$ was traced in different concentrations of FRs from 10 to 50 nM. The increasing of the FR concentration up to 50 nM resulted in the continuous decrease of $i_{p,c}$ to 35.4 μA (Fig. 4b). The decrease of $i_{p,c}$ can be attributed to the retardation of the electron transfer between the electrode surface and electrolyte due to the specific binding of FR proteins with the FA moieties of rGO/FA-Py assemblies in the rGO/FA-Py modified working electrode (Fig. 4c). Therefore, it is estimated that the pteroate heads of FA-Py in the assembly are placed spatially outside of the graphene basal plane, which is a prerequisite for the efficient molecular recognition between FA and FR [18]. The $i_{p,c}$ response of the rGO/FA-Py modified electrode was linear up to the FR concentration of 25 nM. However, it showed a certain saturation of $i_{p,c}$ at the FR concentration of 50 nM, which is estimated to originate from the presence of hardly-accessible FA moieties in the modified electrode towards FRs. The sensitivity of the rGO/FA-Py decorated electrochemical electrode for FRs was evaluated by calculating the limit of detection (LOD). The calculated LOD, where LOD is defined as 3.3 times the standard deviation of the y intercept divided by the slope of the linear calibration fitting [32], was as low as 3.07 nM, which is regarded as the upper limits of quantitation in this study and much lower compared with other reports. For example, the graphene electrode modified with the peptide nanotube-FA hybrid had a detection limit of 8 nM for FRs in a similar electrochemical test [31]. The enhanced performance of rGO/FA-Py modified electrodes might originate from the following characteristics of the rGO/FA-Py assembly: 1) An ultrathin morphology providing a much higher surface area for the binding between FRs on the rGO/FA-Py assemblies. 2) Organo-solubility providing high water resistance during the electrochemical events proceeded in the aqueous media. 3) Preservation of intact pteroate heads in the rGO/FA-Py assembly not providing detrimental effects on the specific binding of FRs on rGO/FA-Py assemblies.

While various fluorescence on/off sensors based on rGO have been demonstrated [33], the facile fluorescence quenching between rGO and FA-Py in this study hampers the application of the rGO/FA-Py assembly as a fluorescence on/off biosensor. To develop efficient fluorescence on/off sensor systems, other types of molecular designs and high dispersion stability in the aqueous media are a prerequisite [34]. In the application of the rGO/FA-Py assembly as an electrochemical biosensor in this study, the robust noncovalent binding of FA-Py molecules on the rGO plate and the extremely poor solubility of the rGO/FA-Py assembly in aqueous media were

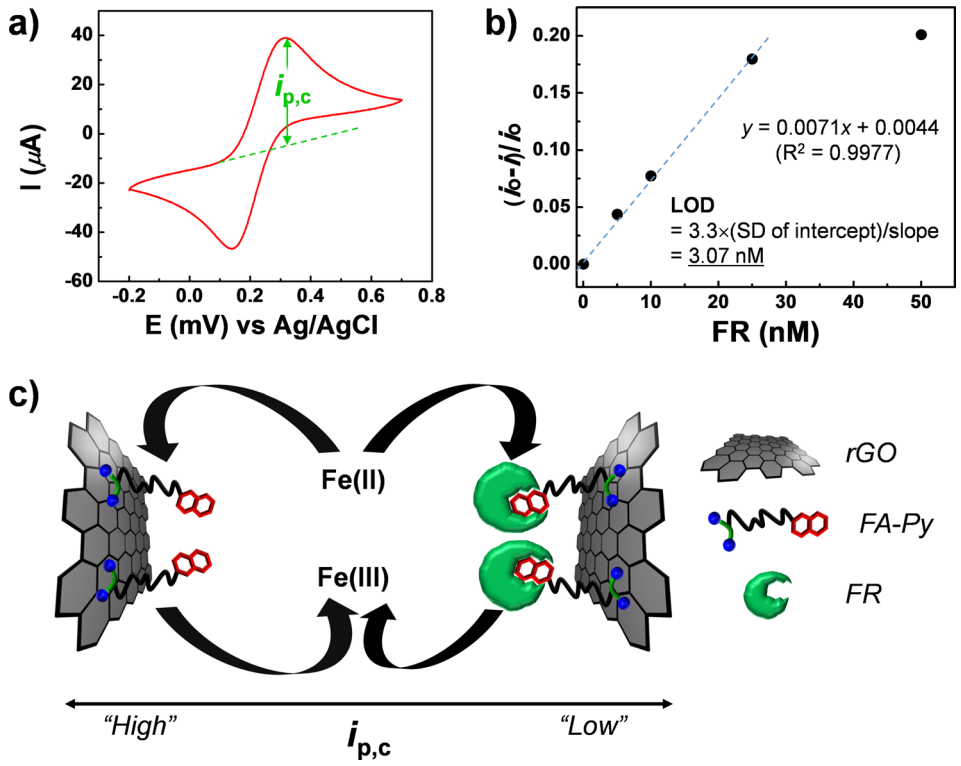

Fig. 4. (a) CV curve of rGO/FA-Py revealed peak current of 39.18 μA, (b) plot of normalized $i_{p,c}$ measured by using cyclic voltammetry using rGO/FA-Py modified working electrodes versus the concentration of FR, and (c) electron transfer according to the accumulation of FR proteins near the working electrode decorated with rGO/FA-Py possessing folate moieties.

synergistically helpful for the electrochemical sensing of FRs in the aqueous media. Through all the electrochemical measurements, the noticeable release of rGO/FA-Py from a working electrode has not been observed, showing that the rGO/FA-Py assembly is highly stable during repeated electrochemical events in CV analysis, probably due to the extremely low water solubility of the rGO/FA-Py assembly.

4. Conclusions

An organo-soluble rGO/FA-Py assembly was easily prepared by the simple mixing and chemical reduction of GO and FA-Py in the mixed solvents of DMF and water. FA-Py molecules played a key role in constructing an organo-dispersible rGO/FA-Py assembly through an π–π interaction between the pyrene moieties of FA-Py and rGO. The resulting rGO/FA-Py assembly revealed a high binding affinity for FRs overexpressed in cancer cells, showing that FA moieties in the assembly are highly bioactive for sensing various physiological events where the specific binding between FA and FR is mediated.

Conflict of Interest

No potential conflict of interest relevant to this article was reported.

Acknowledgements

This research was supported by Radiation Technology R&D program (NRF-2017M2A2A6A01019289) funded by the Ministry of Science, ICT & Future Planning , International Joint Technology Development Project (No. N0002123) funded by the Ministry of Trade, Industry and Energy, and Basic Science Research Program through the National Research Foundation of Korea(NRF) funded by the Ministry of Education(NRF-2018R1A6A1A03023788).

References

[1] Loh KP, Bao Q, Eda G, Chhowalla M. Graphene oxide as a chemically tunable platform for optical applications. Nat Chem, **2**, 1015 (2010). https://doi.org/10.1038/nchem.907.

[2] Balandin AA. Thermal properties of graphene and nanostructured carbon materials. Nat Mater, **10**, 569 (2011). https://dx.doi.org/10.1038/nmat3064.

[3] Kim KS, Zhao Y, Jang H, Lee SY, Kim JM, Kim KS, Ahn JH, Kim P, Choi JY, Hong BH. Large-scale pattern growth of graphene films for stretchable transparent electrodes. Nature, **457**, 706 (2009). https://doi.org/10.1038/nature07719.

[4] Liu J, Tang J, Gooding JJ. Strategies for chemical modification of graphene and applications of chemically modified graphene. J Mater Chem, **22**, 12435 (2012). https://doi.org/10.1039/c2jm31218b.

[5] Chen D, Feng H, Li J. Graphene oxide: preparation, functionalization, and electrochemical applications. Chem Rev, **112**, 6027 (2012). https://doi.org/10.1021/cr300115g.
[6] Chua CK, Pumera M. Chemical reduction of graphene oxide: a synthetic chemistry viewpoint. Chem Soc Rev, **43**, 291 (2014). https://doi.org/10.1039/c3cs60303b.
[7] Englert JM, Dotzer C, Yang G, Schmid M, Papp C, Gottfried JM, Steinrück HP, Spiecker E, Hauke F, Hirsch A. Covalent bulk functionalization of graphene. Nat Chem, **3**, 279 (2011). https://doi.org/10.1038/nchem.1010.
[8] Georgakilas V, Otyepka M, Bourlinos AB, Chandra V, Kim N, Kemp KC, Hobza P, Zboril R, Kim KS. Functionalization of graphene: covalent and non-covalent approaches, derivatives and applications. Chem Rev, **112**, 6156 (2012). https://doi.org/10.1021/cr3000412.
[9] Xu Y, Bai H, Lu G, Li C, Shi G. Flexible graphene films via the filtration of water-soluble noncovalent functionalized graphene sheets. J Am Chem Soc, **130**, 5856 (2008). https://doi.org/10.1021/ja800745y.
[10] Guo Y, Guo S, Ren J, Zhai Y, Dong S, Wang E. Cyclodextrin functionalized graphene nanosheets with high supramolecular recognition capability: synthesis and host−guest inclusion for enhanced electrochemical performance. ACS Nano, **4**, 4001 (2010). https://doi.org/10.1021/nn100939n.
[11] Lee DY, Khatun Z, Lee JH, Lee YK, In I. Blood compatible graphene/heparin conjugate through noncovalent chemistry. Biomacromolecules, **12**, 336 (2011). https://doi.org/10.1021/bm101031a.
[12] Park YJ, Park SY, In I. Preparation of water soluble graphene using polyethylene glycol: comparison of covalent approach and noncovalent approach. J Ind Eng Chem, **17**, 298 (2011). https://doi.org/10.1016/j.jiec.2011.02.027.
[13] Lee DY, Yoon S, Oh YJ, Park SY, In I. Thermo-responsive assembly of chemically reduced graphene and poly(N-isopropylacrylamide). Macromol Chem Phys, **212**, 336 (2011). https://doi.org/10.1002/macp.201000518.
[14] Lee JY, Park YH, Roy AK, Park B, Jang JH, Park SY, In I. Visualization of noncovalent interaction between aliphatic dendrimers and chemically reduced graphene oxide. Chem Lett, **44**, 665 (2015). https://doi.org/10.1246/cl.141158.
[15] Park YH, Park SY, In I. Direct noncovalent conjugation of folic acid on reduced graphene oxide as anticancer drug carrier. J Ind Eng Chem, **30**, 190 (2015). https://doi.org/10.1016/j.jiec.2015.05.021.
[16] Qin W, Li X, Bian WW, Fan XJ, Qi JY. Density functional theory calculations and molecular dynamics simulations of the adsorption of biomolecules on graphene surfaces. Biomaterials, **31**, 1007 (2010). https://doi.org/10.1016/j.biomaterials.2009.10.013.
[17] Wibowo AS, Singh M, Reeder KM, Carter JJ, Kovach AR, Meng W, Ratnam M, Zhang F, Dann CE. Structures of human folate receptors reveal biological trafficking states and diversity in folate and antifolate recognition. Proc Natl Acad Sci U S A, **110**, 15180 (2013). https://doi.org/10.1073/pnas.1308827110.
[18] Chen C, Ke J, Zhou XE, Yi W, Brunzelle J, Li J, Yong EL, Xu EH, Melcher K. Structural basis for molecular recognition of folic acid by folate receptors. Nature, **500**, 486 (2013). https://doi.org/10.1038/nature12327.
[19] Park S, An J, Jung I, Piner RD, An SJ, Li X, Velamakanni A, Ruoff RS. Colloidal suspensions of highly reduced graphene oxide in a wide variety of organic solvents. Nano Lett, **9**, 1593 (2009). https://doi.org/10.1021/nl803798y.
[20] Li D, Müller MB, Gilje S, Kaner RB, Wallace GG. Processable aqueous dispersions of graphene nanosheets. Nat Nanotechnol, **3**, 101 (2008). https://doi.org/10.1038/nnano.2007.451.
[21] Kim H, Abdala AA, Macosko CW. Graphene/polymer nanocomposites. Macromolecules, **43**, 6515 (2010). https://doi.org/10.1021/ma100572e.
[22] Lee M, Lee J, Park SY, Min B, Kim B, In I. Production of graphene oxide from pitch-based carbon fiber. Sci Rep, **5**, 11707 (2015). https://doi.org/10.1038/srep11707.
[23] Yang Q, Pan X. Preparation and characterization of water-soluble single-walled carbon nanotubes by hybridization with hydroxypropyl cellulose derivatives. Ind Eng Chem Res, **49**, 2747 (2010). https://doi.org/10.1021/ie9014149.
[24] Huo C, Chambron JC, Meyer M. Dual emission of a bis(pyrene)-functionalized, perbenzylated β-cyclodextrin. New J Chem, **32**, 1536 (2008). https://doi.org/10.1039/B803144D.
[25] Park YH, Seo JS, Park SY, Lee JH, In I. Facile noncovalent formulation of organo-soluble chemically reduced graphene oxide/semiconducting polymer assembly. Chem Let, **44**, 685 (2015). https://doi.org/10.1246/cl.141206.
[26] Kim J, Cote LJ, Kim F, Huang J. Visualizing graphene based Sheets by fluorescence quenching microscopy. J Am Chem Soc, **132**, 260 (2010). https://doi.org/10.1021/ja906730d.
[27] Swathi RS, Sebastian KL. Long range resonance energy transfer from a dye molecule to graphene has (distance)$^{-4}$ dependence. J Chem Phys, **130**, 086101 (2009). https://doi.org/10.1063/1.3077292.
[28] Zhang X, Hou L, Cnossen A, Coleman AC, Ivashenko O, Rudolf P, van Wees BJ, Browne WR, Feringa BL. One-pot functionalization of graphene with porphyrin through cycloaddition reactions. Chem Eur J, **17**, 8957 (2011). https://doi.org/10.1002/chem.201100980.
[29] Si Y, Samulski ET. Synthesis of water soluble graphene. Nano Lett, **8**, 1679 (2008). https://doi.org/10.1021/nl080604h.
[30] Marcano DC, Kosynkin DV, Berlin JM, Sinitskii A, Sun Z, Slesarev A, Alemany LB, Lu W, Tour JM. Improved synthesis of graphene oxide. ACS Nano, **4**, 4806 (2010). https://doi.org/10.1021/nn1006368.
[31] Castillo JJ, Svendsen WE, Rozlosnik N, Escobar P, Martinez F, Castillo-León J. Detection of cancer cells using a peptide nanotube-folic acid modified graphene electrode. Analyst, **138**, 1026 (2013). https://doi.org/10.1039/c2an36121c.
[32] Radaram B, Mako T, Levine M. Sensitive and selective detection of cesium via fluorescence quenching. Dalton Trans, **42**, 16276 (2013). https://doi.org/10.1039/C3DT52215F.
[33] Shi Y, Huang WT, Luo HQ, Li NB. A label-free DNA reduced graphene oxide-based fluorescent sensor for highly sensitive and selective detection of hemin. Chem Commun, **47**, 4676 (2011). https://doi.org/10.1039/C0CC05518B.
[34] Liu Z, Tian C, Lu L, Su X. A novel aptamer-mediated $CuInS_2$ quantum dots@graphene oxide nanocomposites-based fluorescence "turn off–on" nanosensor for highly sensitive and selective detection of kanamycin. RSC Adv, **6**, 10205 (2016). https://doi.org/10.1039/C5RA22753D.